IMPROVING FULL-CARDIAC CYCLE STRAIN ESTIMATION FROM TAGGED CMR BY ACCURATE MODELING OF 3D IMAGE APPEARANCE CHARACTERISTICS

Matthew Nitzken[1], *Garth Beache*[2], *Ahmed Elnakib*[1], *Fahmi Khalifa*[1], *Georgy Gimel'farb*[3], *Ayman El-Baz*[1]∗

[1]BioImaging Laboratory, Bioengineering Department,University of Louisville, Louisville, KY, USA.
[2]Radiology Department, School of Medicine, University of Louisville, Louisville, KY, USA.
[3]Department of Computer Science, University of Auckland, Auckland, New Zealand.

ABSTRACT

To reduce noise within a tag line, unsharpen tag edges in the spatial domain, and amplify the tag-to-background contrast, a 3D energy minimization framework for the enhancement of tagged Cardiac Magnetic Resonance (CMR) images, that is based on first- and second-order learned visual appearance models, is proposed. The first-order appearance modeling uses an adaptive Linear Combination of Discrete Gaussians (LCDG) to accurately approximate the empirical marginal probability distribution of CMR signals for a given sequence, and to separate the tag and background submodels. It is also used to classify the tag lines and the background. The second-order model considers image sequences as samples of a translation- and rotation-invariant 3D Markov-Gibbs Random Field (MGRF), with multiple pairwise voxel interactions. A 3D energy function for this model is built by using the analytical estimation of the spatiotemporal geometry and the Gibbs potentials of interaction. To improve the strain estimation, through enhancement of the tag and background homogeneity and contrast, the given sequence is adjusted using comparisons to the energy minimizer. Special 3D geometric phantoms, motivated by the statistical analysis of the tagged CMR data, have been designed to validate the accuracy of our approach. Experiments with the phantoms and eight in-vivo data sets have confirmed the high accuracy of functional parameter estimation for the enhanced CMR images when using popular spectral techniques, such as spectral Harmonic Phase (HARP).

Index Terms— Tagged CMR image, tag line, linear combination of Gaussians, Markov random field, appearance model.

1. INTRODUCTION

Tagged cardiac Magnetic Resonance Imaging (MRI) is a well-known technique for detailed and non-invasive visualization of myocardium motion and deformation [1]. Local diseases, such as coronary atherosclerosis, and global conditions, such as heart failure and diabetes, result in wall dysfunction that is manifested on tagged images with full 3D spatial geometric concordance. Cardiac or MR tagging places a pre-specified pattern of temporary markers (called tags) inside soft body tissues, e.g. tag lines are created by patterns of magnetic spin in the tissue being examined, so that the motion in the tissue that is tagged can be measured from the images [2]. This technique complements traditional anatomical images and can capture detailed information about the heart over time. The tag lines allow for the computation of displacement, rotation, and strain of the heart, among others. While traditional MR techniques carry only information about the motion at the boundaries of an object, tagged images allow us to examine the strain and displacement of the interior of the tissue in fine detail [3, 4].

Known methods for analyzing tagged MR images fall into two broad categories: spatial and frequency, or spectral, domain ones. The former identify and use spatial locations of the tag lines in an image to estimate the whole tissue motion and strain using either a model-based or model-free interpolation and differentiation [5, 6]. An established spectral Harmonic Phase (HARP) method, from the second category, computes phase images from sinusoidal tagged MR images by applying bandpass filters in the Fourier domain. The tissue motion field is built by the HARP tracking and is based on the fact that harmonic phases of material points do not change with motion [7, 8].

Corresponding author:- Tel:(502)-852-5092, Fax:(502)-852-6806, E-mail: aselba01@louisville.edu

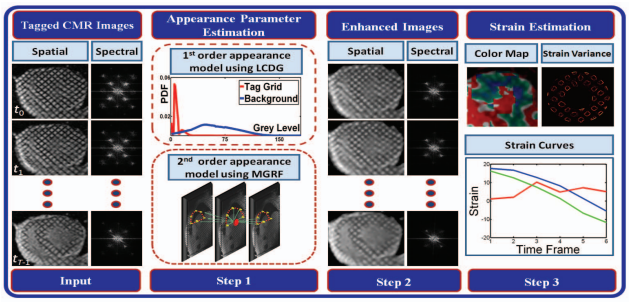


Fig. 1. Block-diagram of the proposed refinement of tagged MR images.

Our research aims to improve the reliability of methods based on spectral domain analysis. HARP analysis, and other very efficient spectral algorithms used for quantitative tag analysis, are often hampered by image noise that affects the spatial tag profiles [9]. When this occurs the assumed motion invariance of the harmonic phases of material points does not hold. The HARP tracking may also fail at points that are close to the tissue boundary, and at points that are approaching or leaving the image plane due to through-plane motion. The failures caused by corrupted images often require the user to manually identify and correct the mistracked points [10, 11]. This is a very time-consuming process, especially in a research study or a clinical examination when large numbers of points are being tracked. Because optimum tagged cardiac MR images images are difficult to obtain, effective image refinement and correction techniques are a prime necessity. To perform the tag data extraction we use the commercial HARP analysis package *Diagnosoft*.

Most commonly, faded tag lines in MR images are refined using histogram equalization. Yang et al. [1] and Liu et al. [2] proposed two different global and local histogram equalization techniques. Due to the high noise levels, many equalized tagged MR images show no reliable and clear distinctions between the tag lines and their background. To reduce this noise influence, Yuan et al. [12] proposed a complex wavelet-decomposition-based bandpass filtering. A tag line map is then built using segmentation, and the image is restored by a pseudo-wavelet reconstruction. The tag lines are finally grouped into pixel clusters and recovered using a snake algorithm. Experimental evaluations showed that while this approach did enhance the tag lines, it was too complex, slow, and insufficiently accurate for efficient clinical use.

An alternative algorithm developed by Li [13] uses peak detection and template matching to classify tag points in the tagged image and determine which of these belong to the tagged lines. While promising results have been shown in experiments, this approach required a considerable body of prior knowledge about the collected data, including tag templates. This prior knowledge could hardly be obtained in a clinical environment because of unavoidable patient motions and the unrestricted placement of the tags. Therefore, its practical usefulness is quite limited.

We propose a more practicable energy minimization based approach for enhancing tagged CMR images. The image noise is reduced and the tag-to-background contrast is enhanced using an original 3D energy function, which accounts for the spatiotemporal pairwise signal interactions, and accurate voxel-wise classification by modeling marginal probability distributions of the tag and background signals. Shown in Fig. 1, the stages of the proposed approach are detailed below.

2. IMAGE REFINEMENT: MODELS AND METHODS

Basic notation. Let $\mathbf{r} = (x, y, t)$ and $\mathbf{R} = [(x, y, t) : x = 0, \ldots, X - 1; y = 0, \ldots, Y - 1, t = 0, \ldots, T - 1]$ denote a 3D point, or voxel with two spatial (x, y) and one time (t) coordinates and a spatiotemporal lattice of the size XYT, respectively. Let $\mathbf{Q} = \{0, \ldots, Q-1\}$ be a finite set of signals (i.e., gray levels intensities). The lattice $\mathbf{R}$ supports 3D CMR image sequences $\mathbf{g} = [g(x, y, t) : (x, y, t) \in \mathbf{R}; g(x, y, t) \in \mathbf{Q}]$, consisting of 2D MR slices taken in successive time instants.

We describe the visual appearance of the tagged CMR images with a 1st-order model of the marginal probability distributions of the tag and background signals and a 2nd-order model of the characteristic voxel-wise and pairwise voxel signal dependencies. The latter are modeled using a generic translation and rotation invariant central-symmetric Markov-Gibbs random field (MGRF) with pairwise voxel potentials that depend on signal differences.

2.1. The 2nd-Order MGRF Appearance Model

A translation- and rotation-invariant generic second-order MGRF of images $\mathbf{g}$ is specified by a certain number, N, of characteristic central-symmetric voxel neighborhoods $\mathbf{n}_\nu$; $\nu = 1, \ldots, N$, on $\mathbf{R}$ shown in Fig. 2. Each neighborhood $\mathbf{n}_\nu$ indicates a family of voxel pairs, $\mathbf{C}_\nu = \{\mathbf{c}_\nu = (\mathbf{r}, \mathbf{r}') : \mathbf{r}' - \mathbf{r} \in \mathbf{n}_\nu;\ \mathbf{r}, \mathbf{r}' \in \mathbf{R}\}$, such that the inter-voxel distances (norms of the coordinate offsets $\mathbf{o} = \mathbf{r}' - \mathbf{r}$) belong to an indexed semi-open interval $[d_{\nu:\min}, d_{\nu:\max})$:

$$d_{\nu:\min} \le \sqrt{(x - x')^2 + (y - y')^2 + (t - t')^2} < d_{\nu:\max} \qquad (1)$$

with the fixed thresholds $d_{\nu:\min}$ and $d_{\nu:\max}$. These neighboring pairs are considered as second-order cliques of the neighborhood graph with nodes in the voxels.

Cliques from the family $\mathbf{C}_\nu$ support the same real-valued Gibbs potential $V_{\boldsymbol{\nu}}(g(\mathbf{r}), g(\mathbf{r}'))$ of the pairwise voxel interaction. To uniformly account for contrast, the potential depends on the absolute intra-clique signal difference: $\Delta = |g(\mathbf{r}) - g(\mathbf{r}')| \in \mathbf{D} = \{0, 1, \ldots, Q - 1\}$. The potential values can be represented as a vector $\mathbf{V}_\nu = [V_\nu(\Delta) : \Delta \in \mathbf{D}]^{\mathsf{T}}$ where T indicates the transposition. The characteristic cliques to be taken into account in the MGRF are stratified into N families, $\{\mathbf{C}_\nu : \nu = 1, \ldots, N\}$. with the potentials $\mathbf{V}_\nu$ and non-intersecting distance intervals: $d_{1:\min} < d_{1:\max} \le d_{2:\min} < \ldots \le d_{N:\min} < d_{N:\max}$.

Such an MGRF has the Gibbs probability distribution [14]:

$$P(\mathbf{g}) = \frac{1}{Z} \exp\left(|\mathbf{R}|\left(\mathbf{V}_{\mathrm{vox}}^{\mathsf{T}}\mathbf{F}(\mathbf{g}) + \sum_{\nu=1}^{N} \rho_\nu \mathbf{V}_\nu^{\mathsf{T}}\mathbf{F}_\nu(\mathbf{g})\right)\right) \qquad (2)$$

where Z is the normalizing factor (the partition function) depending on the potentials $\mathbf{V} = [\mathbf{V}_{\mathrm{vox}}; \mathbf{V}_\nu : \nu = 1, \ldots, N]$ and the neighborhoods $\{\mathbf{n}_\nu : \nu = 1, \ldots, N\}$, and $\rho_\nu = \frac{|\mathbf{C}_\nu|}{|\mathbf{R}|}$ is the relative size of the clique family with respect to the lattice cardinality $|\mathbf{R}| = XYT$, i.e., the relative number of cliques in the family $\mathbf{C}_\nu$. The vectors $\mathbf{F}(\mathbf{g})$ and $\mathbf{F}_\nu(\mathbf{g})$ contain relative empirical frequencies $f(q|\mathbf{g})$ of signals $q \in \mathbf{Q}$ in the voxels and frequencies $f_\nu(\Delta|\mathbf{g})$ of absolute signal differences $\Delta \in \mathbf{D}$ in the cliques from the family $\mathbf{C}_\nu$ for the image $\mathbf{g}$, respectively:

$$\begin{aligned} \mathbf{F}(\mathbf{g}) &= \left[f(q|\mathbf{g}) = \tfrac{|\mathbf{R}_q(\mathbf{g})|}{|\mathbf{R}|};\ \sum_{q\in\mathbf{Q}} f(q|\mathbf{g}) = 1\right] \\ \mathbf{F}_\nu(\mathbf{g}) &= \left[f_\nu(\Delta|\mathbf{g}) = \tfrac{|\mathbf{C}_{\nu:\Delta}(\mathbf{g})|}{|\mathbf{C}_\nu|};\ \textstyle\sum_{\Delta\in\mathbf{D}} f_\nu(\Delta|\mathbf{g}) = 1\right] \end{aligned}$$

where the sublattice $\mathbf{R}_q(\mathbf{g})$ contains all the voxels $\mathbf{r}$, such that $g(\mathbf{r}) = q$ and the subfamily $\mathbf{C}_{\nu:\Delta}(\mathbf{g})$ contains all the cliques $\mathbf{c}_\nu = (\mathbf{r}, \mathbf{r}')$ of this family, such that $|g(\mathbf{r}) - g(\mathbf{r}')| = \Delta$.

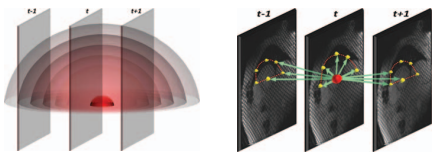


Fig. 2. Central-symmetric 2nd-order 3D neighborhood system.

Analytical first approximations of the maximum likelihood estimates of the potentials in line with [14] are as follows:

$$\begin{aligned} V_{\mathrm{vox}}(q) &= \lambda\left(f(q|\mathbf{g}) - f_{\mathrm{irf}}(q)\right);\ q \in \mathbf{Q}; \\ V_\nu(\Delta) &= \lambda\left(f_\nu(\Delta) - f_{\mathrm{irf}}(\Delta)\right);\ \Delta \in \mathbf{D}; \nu = 1, \ldots, N \end{aligned} \qquad (3)$$

where the common scaling factor λ is also computed analytically, and $f_{\mathrm{irf}}(q) = \frac{1}{Q}$ and $f_{\mathrm{irf}}(\Delta)$ denote the probability of the signal q and the inter-voxel signal difference Δ, respectively, for the independent random field of equiprobable signals:

$$f_{\mathrm{irf}}(\Delta) = \begin{cases} \frac{1}{Q} & \text{if } \Delta = 0 \\ \frac{2(Q-\Delta)}{Q^2} & \text{otherwise} \end{cases}$$

2.2. The 1st-Order LCDG Appearance Model

A discrete Gaussian (DG) $\boldsymbol{\Psi}_\theta = (\psi(q|\theta) : q \in \mathbf{Q})$ is defined [15] as a discrete probability distribution with Q components obtained by integrating a continuous 1D Gaussian density $\varphi(q)\theta) = (\sigma * \sqrt{2\pi})^{-1} * \exp\left(-\frac{(q-\mu)^2}{2\sigma^2}\right)$ with parameters $\theta = (\mu, \sigma)$, where μ is the mean and σ^2 is the variance, over Q intervals related to the successive signal values in $\mathbf{Q}$: if $\Phi_\theta(q) = \int_{-\infty}^{q} \varphi(z|\theta)dz$ is the cumulative Gaussian probability function, then $\psi(0|\theta) = \Phi_\theta(0.5)$, $\psi(q|\theta) = \Phi_\theta(q + 0.5) - \Phi_\theta(q - 0.5)$ for $q = 1, \ldots, Q - 2$, and $\psi(Q - 1|\theta) = 1 - \Phi_\theta(Q - 1.5)$.

To enhance the tag-to-background contrast, the empirical marginal 1D signal distribution for the CMR image to be refined is accurately approximated with a Linear Combination of Discrete Gaussians (LCDG) $\mathbf{P}_{\mathbf{w},\boldsymbol{\Theta}} = [p_{\mathbf{w},\boldsymbol{\Theta}}(q) : q \in \mathbf{Q}]$; $\sum_{q\in\mathbf{Q}} p_{\mathbf{w},\boldsymbol{\Theta}}(q) = 1$, with two positive dominant and multiple sign-alternate subordinate DGs:

$$p_{\mathbf{w},\boldsymbol{\Theta}}(q) = \sum_{k=1}^{K_{\mathrm{p}}} w_{\mathrm{p}:k}\psi(q|\theta_{\mathrm{p}:k}) - \sum_{l=1}^{K_{\mathrm{n}}} w_{\mathrm{n}:l}\psi(q|\theta_{\mathrm{n}:l}) \qquad (4)$$

where K_{p}; $K_{\mathrm{p}} \ge 2$, and K_{n}; $K_{\mathrm{n}} \ge 0$, are total numbers of the positive and negative DGs, and $\mathbf{w} = [w_{\mathrm{p}:k}, w_{\mathrm{n}:l}]$ are the non-negative weights that meet the obvious constraint $\sum_{k=1}^{K_{\mathrm{p}}} w_{\mathrm{p}:k} - \sum_{l=1}^{K_{\mathrm{n}}} w_{\mathrm{n}:l} = 1$. The subordinate DGs approximate closely the deviations of the empirical distribution from the conventional mixture of the dominant positive DGs.

This initial LCDG model is built and separated into the two LCDG submodels of the tag lines and their background, respectively, with the Expectation-Maximization(EM) based techniques introduced in [15]. Given the number K of the dominant DGs (here, $K = 2$), the numbers $K_{\mathrm{p}} - K$ and K_{n} of the subordinate components, as well as the parameters $\mathbf{w}$, $\boldsymbol{\Theta}$ (i.e., the weights, the means, and the variances) of all the DGs, are first estimated using a sequentially initialized EM-based algorithm that produces a close initial LCDG-approximation of the empirical distribution. Then under the fixed number of components, K_{p} and K_{n}, all the other parameters are refined with an EM algorithm that is modified to account for sign-alternate components. The refined LCDG model is finally partitioned into two LCDG submodels $\mathbf{p}_{\mathrm{vox}:\alpha} = [p_{\mathrm{vox}:\alpha}(q) : q \in \mathbf{Q}]$, one per class $\alpha \in \{\mathrm{tag}, \mathrm{background}\}$, by associating the subordinate DGs with the dominant components in such a way that the misclassification rate is minimal.

2.3. Energy Minimization to Enhance Tagged CMR Images

We adjust a tagged CMR image $\mathbf{g}$ by searching with a voxel-wise Iterative Conditional Mode (ICM) relaxation for a local minimum of the Gibbs energy function for the second-order MGRF appearance model:

$$\widehat{\mathbf{g}} = \arg\min_{\mathbf{g}\in\mathbf{Q}^{XYT}} \left\{\mathbf{V}_{\mathrm{vox}}^{\mathsf{T}}\mathbf{F}(\mathbf{g}) + \sum_{\nu=1}^{N} \rho_\nu \mathbf{V}_\nu^{\mathsf{T}}\mathbf{F}_\nu(\mathbf{g})\right\} \qquad (5)$$

where the probability vectors $\mathbf{F}_{\mathrm{vox}}(\mathbf{g})$ and $\mathbf{F}_\nu(\mathbf{g})$ are collected over the generated tagged CMR image sequence. To enhance the tag-background contrast, each estimated signal value $\widehat{g}(\mathbf{r})$; $\mathbf{r} \in \mathbf{R}$, is classified as belonging to either the tag line or the background using the first-order LCDG model. Then the voxels are nudged towards their proper grouping by incrementing or decrementing their signals by a small value δ in accordance with the discriminant threshold.

The basic steps of the proposed enhancement are as follows:

1. Find the empirical marginal probability distribution by normalizing the signal histogram collected over a given tagged CMR image sequence.
2. Use the LCDG modeling of Section 2.2 to estimate the LCDG-submodels approximating the marginal signal distributions for the tag lines and the background.
3. Use these LCDG-submodels to evaluate the discriminant threshold τ, which minimizes the error of classification of the tag and background voxels by their signal values.
4. Use Eq. (3) in Section 2.1, for the given sequence, to estimate the first- and second-order potentials, $\mathbf{V}_{\text{vox}}$ and $\mathbf{V}$, of the MGRF appearance model.
5. Use the ICM, starting from the given sequence $\mathbf{g}$, to estimate a sequence $\widehat{\mathbf{g}}$, which minimizes the energy of Eq. (5).
6. Compare the estimated voxel signals $\widehat{g}(\mathbf{r})$; $\mathbf{r} \in \mathbf{R}$, to the threshold τ found at Step 3 and add or subtract the bias δ from the estimated gray level value if the latter is higher or lower than the threshold, respectively.

3. EXPERIMENTAL RESULTS

The effectiveness of the proposed approach was tested on both synthetic phantom images and in-vivo data by analyzing the strain of the data sets using the HARP technique and quantifying the performance with two indexes: (*i*) the ability to restore strain slopes for synthetic phantoms and (*ii*) the homogeneity of the strain variance in the data.

3.1. Validation on Synthetic Phantoms

The synthetic phantoms were constructed using a descriptive model [16, 17] that accounts for physiological features and response during the cardiac cycle of the left ventricle (LV). A geometric transformation that covers shearing, rotation, translation, torsion, and compression of the LV is used in the model to describe the LV motion by mapping each location (i.e.,a material point) defined in the LV model to a corresponding spatial point at a certain time instant. Using this transformation, an inverse motion map is calculated analytically, and is used to establish correspondences between two points at any two time instants. This allows for the simulation of tagged MR image sequences.

To obtain the phantoms, a motion transformation is applied to a generated 3D LV model. Then, an image is generated by selecting an image plane that intersects the LV and assigning every point on the image plane a value that depends on whether the point lies inside or outside the LV wall. A phantom constructed using this model is exemplified in Fig. 3 (a). Realistic images are simulated by corrupting the phantom images with Gaussian noise using the signal-to-noise Ratio (SNR) of 3.18 dB and 2.58 dB, as shown in Fig. 3 (b) and (c), respectively.

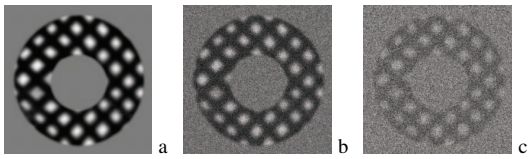


Fig. 3. Original phantom (a) and two Gaussian corruption levels with the SNR of 3.18 dB (b) and 2.58 dB (c).

In cardiac strain analysis, the slope of the contraction phase of the cardiac cycle is a very important part of the strain curve, i.e., cardiac systolic performance index, or rate of peak contraction. Therefore, the accurate recovery of this slope is an important index of a tagged MR restoration algorithm. To measure the effect of the additive noise on the calculated strain. the absolute strain error, i.e.,the difference between the slopes of the noisy data analyzed and the ground truth, was calculated for the phantom images. The calculation was done using the HARP technique and the Euler strain measurements. After applying the proposed processing approach, the approximate absolute strain error for the noisy phantom images was reduced from 94% to 35.7%. Figure 4 visually compares the strain in the original, corrupted, and enhanced phantoms.

The actual strain slopes calculated for the original, corrupted, and our enhanced phantoms are compared in Fig. 5. As is expected and demonstrated in Fig. 5, the strain values are decreasing linearly with time during

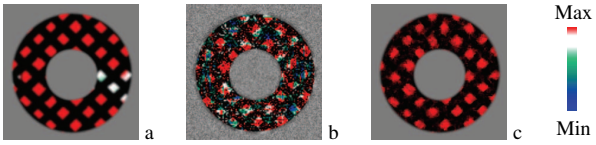


Fig. 4. Visualization of the strain on the phantom for the (a) original, (b) corrupted and (c) enhanced images. Coloring indicates the strain percentage. Note how the strain is largely recovered in the enhanced image.

the contraction phase of the cardiac cycle. That the slope profiles for the enhanced and ground truth images are very similar clearly demonstrates the capabilities of the proposed approach to facilitate the accurate recovery of the strain for the tagged MR data. Visually this is also evident from the color uniformity of the images in Fig. 4, (a) and (c). At the same time, the color scatter over the noisy phantom in Fig. 4, (b), illustrates the failure of the HARP-based strain calculations under the large corrupting noise.

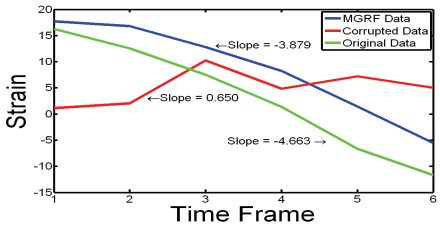


Fig. 5. Strains calculated at the contraction phase of the cardiac cycle for the original, corrupted, and enhanced phantom images. Note that the slope is made unreliable, and does not approximate the actual underlying data in the corrupted phantom, indicating that the HARP analysis cannot track the strain at all in this image. After applying our enhancement to the corrupted image, the slope, is largely recovered.

For accurate computations in the spectral domain, the HARP technique requires that the information reside predominately within the central peak and first side lobes. The Fourier spectral representations of the noisy and enhanced phantom images in Fig. 6 justify the high accuracy of recovering the strain slope using the proposed approach. As shown in Fig 6 (a), it is the increased power scatter distributing information in the outer side lobes of the Fourier domain, for the corrupted phantom image, that greatly affects the accuracy of the HARP analysis.

Our enhancement reduces the scatter in the outer side lobes and emphasizes the main lobe and first side lobes in the Fourier image spectral domain, which therefore makes the HARP analysis much more accurate and robust. In total, our approach gives $265\% \pm 20\%$ of noise reduction in the side lobes of the phantom image spectrum. Table 1 summarizes the noise reduction results for the phantom data.

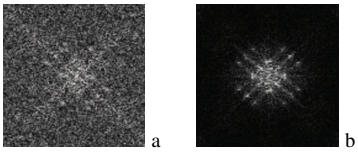


Fig. 6. Fourier spectra of the (a) corrupted and (b) enhanced phantom images.

Another important aspect of the proposed approach is the ability to restore strain homogeneity in the tagged MR images. This is directly related to HARP tracking and the ability to restore the strain slopes (the improved homogeneity leads to the improved strain slope). Based on biomechanical models of the heart tissue as a continuous material, neighboring voxels in a heart should have similar strains, and the strain does not randomly occur in every individual voxel, the variance in strain (homogeneity) in actual tagged MR image sequences should be low. This should hold true in any given continuous region, even in the presence of injury. To justify our approach, after the strains of each image were extracted, the strain homogeneity of the phantoms was calculated in terms of the strain variance in 7×7 windows across the phantom images. Differences between the mean strain homogeneity in Table 3 before and after the image en-

hancement are statistically significant by the unpaired t-test, so that our approach robustly improves both the strain slope and homogeneity.

	Mean	St.dev.
Before	0.17	0.012
After	0.58	0.019
% imp.	**265%**	**20%**

Table 1. The ratio of the main lobe's spectral power for the corrupted phantom data set before and after the enhancement with the percentage of improvement.

	Mean	St.dev.
Before	1.31	0.18
After	1.86	0.19
% imp.	**43%**	**9.2%**

Table 2. Spectral main lobe power for the in-vivo data before and after the processing with the percentage of improvement.

	Before	After
Mean	0.024	0.0092
St.dev.	$2.9 \cdot 10^{-14}$	$1.8 \cdot 10^{-15}$
P-Value	$< 10^{-4}$	

Table 3. Strain homogeneity before and after the enhancement.

Pixel-wise parametric (color-coded) maps in Fig. 7 for the original, corrupted, and enhanced phantoms help to assess visually the improvement in the strain homogeneity: the brighter the area, the larger the local strain variance. Our approach largely recovers the strain variance profile of the original image.

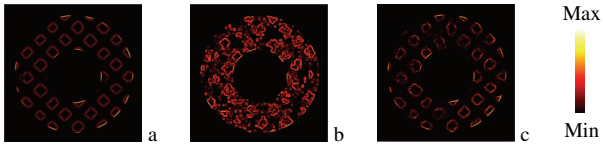


Fig. 7. Color-coded strain variance maps for the (a) original, (b) corrupted, and (c) enhanced phantom. The corrupted image shows an increased amount of variance and less discrete elements.

3.2. Results for In-vivo Data

To test the realistic performance, the proposed approach has been applied to eight in-vivo data sets. Shown in Fig. 8, the results before and after enhancing one of the test images are similar to those for the phantom data. Additionally, the spectra shows a considerable noise reduction in the side lobes; see Fig. 8 (c) and (d).

As shown in Table 2, the proposed approach can significantly reduce various levels of the noise, e.g., the noise reduction of $42.6\% \pm 9.3\%$ in the spectral side lobes for all of the eight in-vivo data sets that took part in these experiments. Furthermore, similarly to the phantom data, the overall strain homogeneity of the image clearly increases as well. Figure 9 demonstrates an in-vivo image before and after the proposed enhancement, showing improved continuous areas.

3.3. Computational Efficiency

The processing time of the entire HARP analysis is only slightly increased with the proposed approach. The average processing time required for processing one 256×256 DICOM image was 9.4 ± 0.2 seconds, and a typical data set, of 15 MR images, was on average 145 seconds. Unlike other alternatives, our technique requires no user input or apriori model templates, and all of the parameters are automatically learned from a given sequence of CMR images. The overall data analysis time is therefore reduced and the analysis is made more robust due to the elimination of possible human errors.

4. CONCLUSION

Many methods exist currently for analyzing tagged MR images. Spectral techniques, such as HARP, are arguably the most clinically useful for the fast analysis of cardiac strain data. While many approaches have been proposed to improve tagged MR images as a whole, to the best of our knowledge ours is the first to focus directly on improving the spectral quality of images in order to directly facilitate spectral analysis. Our results show that probabilistic first- and second-order models of spatiotemporal images can contribute directly to image denoising in the spectral domain, and therefore improve spectral techniques.

Our LCDG and MGRF based modeling of the tagged MR images in the spatiotemporal domain is capable of recovering strain slopes, which

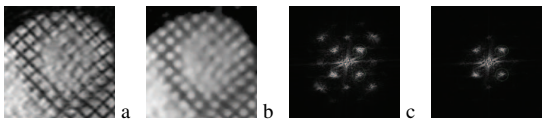


Fig. 8. An in-vivo data set: the original spatial (a) and processed (b) images and their Fourier spectra (c), (d). The spectral noise is notably reduced by the proposed image enhancement.

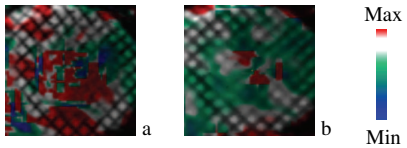


Fig. 9. In-vivo data strain maps before (a) and after (b) our enhancement. Note that the variability in strain has been largely reduced and the final homogeneity is notably increased.

are an important clinical feature of strain curves. Additionally, it improves the main-to-side-lobe ratio in the Fourier spectra, which measures the noise reduction in the spectral domain. Simultaneously, the proposed approach improves the strain homogeneity. These image improvements ensure a more efficient and robust estimation of functional parameters with today's spectral analysis tools. In total, our approach can lead to more accurate clinical cardiac measurements and evaluations, while it adds only a minimal amount of time to HARP image analysis. Thus, in addition to restoring strain slopes, reducing spectral noise, and improving strain homogeneity, the proposed method can provide clinicians with more accurate image data to make judgements for patients.

5. REFERENCES

[1] Y. Yang *et al.*, "Tagged cardiac mr image segmentation by contrast enhancement and texture analysis," pp. 4–210 –4–214, Aug. 2009.

[2] X. Liu and J. Prince, "Shortest path refinement for motion estimation from tagged mr images," *IEEE TMI,*, vol. 29, no. 8, pp. 1560 –1572, Aug. 2010.

[3] L. Axel and L. Dougherty, "MR imaging of motion with spatial modulation of magnetization," *Radiology*, vol. 171, pp. 841–45, Jun 1989.

[4] ——, "Heart wall motion: improved method of spatial modulation of magnetization for MR imaging," *Radiology*, vol. 172, pp. 349–350, Aug 1989.

[5] J. Denney, T.S. and J. Prince, "Reconstruction of 3-d left ventricular motion from planar tagged cardiac mr images: an estimation theoretic approach," *IEEE TMI*, vol.14, no.4, pp.625 –35, Dec 1995.

[6] W. S. Kerwin and J. L. Prince, "Cardiac material markers from tagged MR images," *Med Image Anal*, vol.2, pp.339–353, Dec 1998.

[7] N. F. Osman and J. L. Prince, "Visualizing myocardial function using HARP MRI," *Phys Med Biol*, vol. 45, pp. 1665–1682, Jun 2000.

[8] N. Osman, E. McVeigh *et al.*, "Imaging heart motion using harmonic phase mri," *IEEE TMI*, vol. 19, no. 3, pp. 186 –202, 2000.

[9] X. Liu, E. Murano *et al.*, "Harp tracking refinement using seeded region growing," pp. 372 –375, April 2007.

[10] X. Liu, M. Stone *et al.*, "Tracking tongue motion in three dimensions using tagged mr image," pp. 1372 –1375, April 2006.

[11] W. Levine, C. Essex-Torcaso *et al.*, "A nonlinear incompressible model of the human tongue," *SIAM news*, vol. 39, no. 2, 2006.

[12] X. Yuan, J. Zhang *et al.*, "A multiresolution method for tagline detection and indexing," *Information Technology in Biomedicine, IEEE*, vol. 14, no. 2, pp. 507 –513, March 2010.

[13] J. Li, "Tag line tracking and cardiac motion modeling from tagged mri." 2006.

[14] G. Gimel'farb, *Image textures and Gibbs random fields*. Kluwer Academic Pub, 1999, vol. 16.

[15] A. El-Baz and G. Gimel'farb, "Em based approximation of empirical distributions with linear combinations of discrete gaussians," vol. 4, pp. IV –373 –IV –376, 16 2007-Oct. 19 2007.

[16] T. Arts, W. C. Hunter *et al.*, "Description of the deformation of the left ventricle by a kinematic model," *J Biomech*, vol. 25, pp. 1119–1127, Oct 1992.

[17] E. Waks, J. Prince *et al.*, "Cardiac motion simulator for tagged mri," in *Math. Methods in Biomed. Image Analysis*, Jun 1996, pp. 182–91.